

Investigation of the Effects of Constitutive Equations on the Free Vibration Behavior of Single-Celled Thin-Walled Composite Beams

H. R. OVESY and P. KHANEH MASJEDI

Aerospace Engineering Department and the Center of Excellence in Computational Aerospace Engineering, Amirkabir University of Technology, Tehran, Iran

Received 23 November 2011; accepted 26 June 2012.

An investigation of the free vibration behavior of thin-walled composite box-beams is carried out by considering different assumptions in the constitutive equations. Within the present model some non-classical effects, such as restrained warping and transverse shear, are incorporated. Free vibration results are validated against experimental and numerical results, which are available in the literature. The natural frequencies obtained based on the different assumptions of constitutive equations are compared, and it is revealed that these assumptions play an important role in the proper treatment of the free vibration behavior of torsion-bending coupled composite beams. The results obtained based on the proposed constitutive equations are demonstrated to have a good agreement with the finite element results as far as the lower natural frequencies of the beams are concerned.

Keywords: composite beam, thin-walled beam, constitutive equations, free vibration, restrained warping, cross-sectional deformation

1. Introduction

The enhancement of the theory of thin-walled composite beams has notably drawn the attention of many researchers in the past two decades. It has been revealed that in order to properly treat the behavior of thin-walled composite beams, a number of nonclassical effects, such as restrained warping, transverse shear, and also the mechanisms of structural couplings, have to be carefully considered.

Song and Librescu [1] have proposed a model in which the effects of restrained warping and transverse shear on the vibration behavior of composite beams are studied. By including these effects, the predicted values of the natural frequencies have become lower than the corresponding values obtained by neglecting restrained warping effects. In a model developed by Chandra and Chopra [2], it is suggested that the variation of shear stiffness along the contour of a cross-section has a significant influence on the warping and twist characteristic of a composite beam. Volovoi and Hodges [3] have used an asymptotically correct linear theory for com-

posite thin-walled beams. They have revealed that the inclusion of hoop bending moment and shell bending is important for a proper prediction of torsional stiffness of a number of thin-walled composite beams. The latter finding is used by Jung et al. [4] in order to subsequently suggest a so-called mixed method, which combines the force and displacement approaches in a unified form. They have then achieved similar results to those of Volovoi and Hodges [3]. Qin and Librescu [5] have validated the model developed earlier in Song and Librescu [1] against experimental data. They have shown that the static and dynamic behaviors predicted by this refined model are in good agreement with experimental data and other analytical models. Suresh and Nagaraj [6], in a comprehensive comparison between experimental and analytical results, have revealed that their proposed model, in which the refined warping function and higher shear deformation theory are considered, can predict the static and dynamic behavior of thin-walled composite beams efficiently. They suggested that the way the warping is modeled has a significant role in a correct treatment of thin-walled composite beams.

The model that is used in the current study is mainly based on the works by Song and Librescu [1] and Qin and Librescu [5] with some modifications in the constitutive equations. It will be shown that these modifications can significantly influence the free vibration behavior of single-celled thin-walled composite beams.

Address correspondence to H. R. Ovesy, Aerospace Engineering Department and the Center of Excellence in Computational Aerospace Engineering, Amirkabir University of Technology, 424 Hafez Avenue, P.O. 15875-4413, Tehran, Iran. E-mail: Ovesy@aut.ac.ir

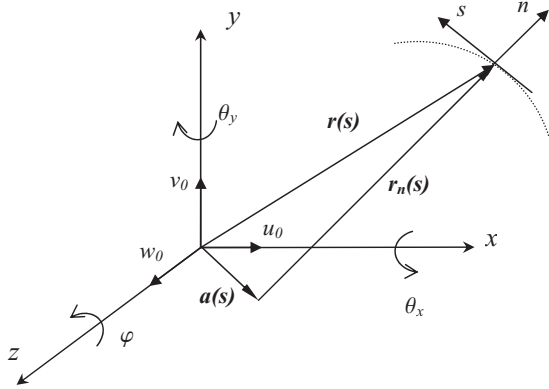


Fig. 1. Coordinate systems and kinematic variables for the beam model.

2. Theoretical Developments

2.1. Kinematics

For completeness, the previous model by Song and Librescu [1] and Qin and Librescu [5], on which the current study is mainly based, is presented below.

The geometric configuration and the chosen coordinate system are depicted in Figures 1 and 2.

In order to model a single-celled cross-section fiber-reinforced thin-walled beam, the following assumptions are adopted [5]:

- (1) The cross-sections do not deform in their own planes.
- (2) Transverse shear effects are incorporated. In addition, it is stipulated that the transverse shear strains, γ_{xz} and γ_{yz} , are uniform over the cross-sections.
- (3) In addition to the warping displacement along the mid-line contour (referred to as primary warping), the off mid-line contour warping (referred to as the secondary warping) is also incorporated.
- (4) It is assumed that over the cross-section, σ_{nn} and N_{sn} are negligibly small when deriving the stress-strain constitutive law.

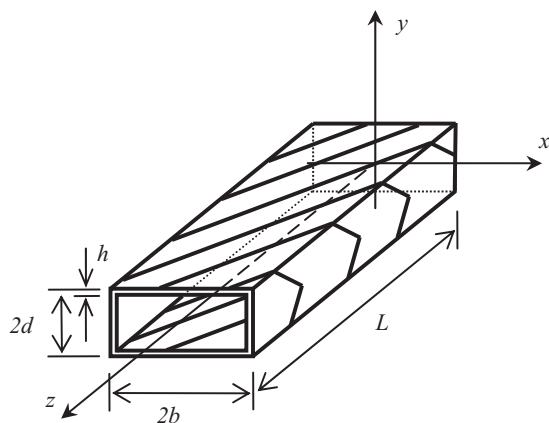


Fig. 2. The geometry of the thin-walled composite box-beam (CAS lay-up, $\theta(y) = -\theta(-y)$, $\theta(x) = -\theta(-x)$).

- (5) The deformations are small and linear elasticity theory is used.

Based on the latter assumptions, the following displacements and strains that contribute to the potential energy are adopted [5]:

$$u(x, y, z, t) = u_0(z, t) - y\varphi(z, t), \tag{1a}$$

$$v(x, y, z, t) = v_0(z, t) + x\varphi(z, t), \tag{1b}$$

$$w(s, z, n, t) = w_0(z, t) + \theta_y(z, t) \left(x + n \frac{dy}{ds} \right) + \theta_x(z, t) \left(y - n \frac{dx}{ds} \right) - \varphi'(z, t) \{ \bar{F}(s) + \bar{\bar{F}}(n, s) \}, \tag{1c}$$

where

$$\bar{F}(s) = \int_0^s [r_n(s) - \psi(s)] ds, \tag{2a}$$

$$\bar{\bar{F}}(n, s) = -na(s), \tag{2b}$$

in which $\bar{F}(s)$ and $\bar{\bar{F}}(n, s)$ are referred to as primary and secondary warping functions and $()'$ denotes the derivative with respect to z and

$$r_n(s) = x \frac{dy}{ds} - y \frac{dx}{ds}, \tag{3a}$$

$$a(s) = x \frac{dx}{ds} + y \frac{dy}{ds}, \tag{3b}$$

$$\psi = \frac{\oint r_n ds}{\oint ds}, \tag{3c}$$

$$\theta_x(z, t) = \gamma_{yz} - v'_0, \tag{4a}$$

$$\theta_y(z, t) = \gamma_{xz} - u'_0. \tag{4b}$$

Spanwise strain can be written as follows:

$$\epsilon_{zz}(s, z, n, t) = \epsilon_{zz}^{(0)}(s, z, t) + n\epsilon_{zz}^{(1)}(s, z, t), \tag{5a}$$

where

$$\epsilon_{zz}^{(0)}(s, z, t) = w'_0(z, t) + \theta'_y(z, t)x(s) + \theta'_x(z, t)y(s) - \varphi''(z, t)\bar{F}(s), \tag{5b}$$

$$\epsilon_{zz}^{(1)}(s, z, t) = \theta'_y(z, t) \frac{dy}{ds} - \theta'_x(z, t) \frac{dx}{ds} + \varphi''(z, t)a(s), \tag{5c}$$

and tangential and transverse shear strains are as follows:

$$\gamma_{sz} = \gamma_{sz}^{(0)} + \psi \varphi', \tag{6a}$$

$$\gamma_{nz} = (\theta_y + u'_0) \frac{dy}{ds} - (\theta_x + v'_0) \frac{dx}{ds}, \tag{6b}$$

where

$$\gamma_{sz}^{(0)} = (\theta_x + v'_0) \frac{dy}{ds} + (\theta_y + u'_0) \frac{dx}{ds}. \tag{6c}$$

2.2. Constitutive Equations

Considering a thin-walled composite beam consisting of N laminates, the constitutive equations for the k th lamina can be shown to be as follows:

$$\begin{Bmatrix} \sigma_{ss} \\ \sigma_{zz} \\ \sigma_{nn} \\ \sigma_{zn} \\ \sigma_{sn} \\ \sigma_{sz} \end{Bmatrix}_{(k)} = [C]_{(k)} \begin{Bmatrix} \epsilon_{ss} \\ \epsilon_{zz} \\ \epsilon_{nn} \\ \gamma_{zn} \\ \gamma_{sn} \\ \gamma_{sz} \end{Bmatrix}_{(k)}, \tag{7a}$$

where $[C]_{(k)}$ is the stiffness matrix of the k th lamina and

$$[C]_{(k)} = \begin{bmatrix} C_{11} & C_{12} & C_{13} & 0 & 0 & C_{16} \\ C_{12} & C_{13} & C_{23} & 0 & 0 & C_{26} \\ C_{13} & C_{23} & C_{33} & 0 & 0 & C_{36} \\ 0 & 0 & 0 & C_{44} & C_{45} & 0 \\ 0 & 0 & 0 & C_{45} & C_{55} & 0 \\ C_{16} & C_{26} & C_{36} & 0 & 0 & C_{66} \end{bmatrix}_{(k)}. \tag{7b}$$

where the stiffness coefficients C_{ij} are defined in Appendix A of Librescu and Song [7].

As mentioned before, assuming that the σ_{nn} is negligible compared with the other stress components, i.e., $\sigma_{nn} = 0$, the following expression for the transverse normal strain can be extracted:

$$\epsilon_{nn} = -\frac{C_{13}}{C_{33}}\epsilon_{ss} - \frac{C_{23}}{C_{33}}\epsilon_{zz} - \frac{C_{36}}{C_{33}}\gamma_{sz}. \tag{8}$$

As a result, the constitutive equations can be written as below:

$$\begin{Bmatrix} \sigma_{ss} \\ \sigma_{zz} \\ \sigma_{zn} \\ \sigma_{sn} \\ \sigma_{sz} \end{Bmatrix}_{(k)} = [\bar{Q}]_{(k)} \begin{Bmatrix} \epsilon_{ss} \\ \epsilon_{zz} \\ \gamma_{zn} \\ \gamma_{sn} \\ \gamma_{sz} \end{Bmatrix}_{(k)}, \tag{9a}$$

where $[\bar{Q}]_{(k)}$ is the matrix of transformed reduced elastic coefficients and is given by:

$$[\bar{Q}]_{(k)} = \begin{bmatrix} \bar{Q}_{11} & \bar{Q}_{12} & 0 & 0 & \bar{Q}_{16} \\ \bar{Q}_{21} & \bar{Q}_{22} & 0 & 0 & \bar{Q}_{26} \\ 0 & 0 & \bar{Q}_{44} & \bar{Q}_{45} & 0 \\ 0 & 0 & \bar{Q}_{54} & \bar{Q}_{55} & 0 \\ \bar{Q}_{61} & \bar{Q}_{62} & 0 & 0 & \bar{Q}_{66} \end{bmatrix}_{(k)}, \tag{9b}$$

where

$$\bar{Q}_{ij} = C_{ij} - \frac{C_{i3}C_{j3}}{C_{33}} = \bar{Q}_{ji}, \quad (i, j = 1, 2, 6), \tag{9c}$$

$$\bar{Q}_{lm} = C_{lm}, \quad (l, m = 4, 5). \tag{9d}$$

Toward obtaining the constitutive equations of the thin-walled composite beam, the stress resultants are defined as:

(a) The in-plane stress resultants:

$$\begin{Bmatrix} N_{ss} \\ N_{zz} \\ N_{sz} \end{Bmatrix} = \sum_{k=1}^N \int_{n_{(k-1)}}^{n_{(k)}} \begin{Bmatrix} \sigma_{ss} \\ \sigma_{zz} \\ \sigma_{sz} \end{Bmatrix}_{(k)} dn. \tag{10a}$$

(b) The transverse shear stress resultants:

$$\begin{Bmatrix} N_{zn} \\ N_{sn} \end{Bmatrix} = \sum_{k=1}^N \int_{n_{(k-1)}}^{n_{(k)}} \begin{Bmatrix} \sigma_{zn} \\ \sigma_{sn} \end{Bmatrix}_{(k)} dn. \tag{10b}$$

(c) The out-of-plane stress resultants:

$$\begin{Bmatrix} M_{ss} \\ M_{zz} \\ M_{sz} \end{Bmatrix} = \sum_{k=1}^N \int_{n_{(k-1)}}^{n_{(k)}} \begin{Bmatrix} \sigma_{ss} \\ \sigma_{zz} \\ \sigma_{sz} \end{Bmatrix}_{(k)} ndn. \tag{10c}$$

In the above equations, $n_{(k)}$ and $n_{(k-1)}$ denote the distances from the middle surface of the cross-section to the upper and lower surface of the k th layer and N is the number of layers.

Considering Eqs. (9) and (10) and assuming that the transverse shear stress resultants, M_{zn} and M_{sn} , are negligible, the constitutive equations for a thin-walled composite beam can be derived as:

$$\begin{Bmatrix} N_{ss} \\ N_{zz} \\ N_{sz} \end{Bmatrix} = \begin{bmatrix} A_{11} & A_{12} & A_{16} \\ A_{12} & A_{22} & A_{26} \\ A_{16} & A_{26} & A_{66} \end{bmatrix} \begin{Bmatrix} \epsilon_{ss}^{(0)} \\ \epsilon_{zz}^{(0)} \\ \gamma_{sz} \end{Bmatrix} + \begin{bmatrix} B_{11} & B_{12} & B_{16} \\ B_{12} & B_{22} & B_{26} \\ B_{16} & B_{26} & B_{66} \end{bmatrix} \begin{Bmatrix} \epsilon_{ss}^{(1)} \\ \epsilon_{zz}^{(1)} \\ 0 \end{Bmatrix}, \tag{11a}$$

$$\begin{Bmatrix} M_{ss} \\ M_{zz} \\ M_{sz} \end{Bmatrix} = \begin{bmatrix} B_{11} & B_{12} & B_{16} \\ B_{12} & B_{22} & B_{26} \\ B_{16} & B_{26} & B_{66} \end{bmatrix} \begin{Bmatrix} \epsilon_{ss}^{(0)} \\ \epsilon_{zz}^{(0)} \\ \gamma_{sz} \end{Bmatrix} + \begin{bmatrix} D_{11} & D_{12} & D_{16} \\ D_{12} & D_{22} & D_{26} \\ D_{16} & D_{26} & D_{66} \end{bmatrix} \begin{Bmatrix} \epsilon_{ss}^{(1)} \\ \epsilon_{zz}^{(1)} \\ 0 \end{Bmatrix}, \tag{11b}$$

$$\begin{Bmatrix} N_{zn} \\ N_{sn} \end{Bmatrix} = \begin{bmatrix} A_{44} & A_{45} \\ A_{45} & A_{55} \end{bmatrix} \begin{Bmatrix} \gamma_{zn} \\ \gamma_{sn} \end{Bmatrix}, \tag{11c}$$

where A_{ij} , B_{ij} , and D_{ij} are defined as:

$$A_{ij} = \sum_{k=1}^N \int_{n_{(k-1)}}^{n_{(k)}} \bar{Q}_{ij}^{(k)} dn, \quad (12a)$$

$$B_{ij} = \sum_{k=1}^N \int_{n_{(k-1)}}^{n_{(k)}} \bar{Q}_{ij}^{(k)} n dn, \quad (12b)$$

$$D_{ij} = \sum_{k=1}^N \int_{n_{(k-1)}}^{n_{(k)}} \bar{Q}_{ij}^{(k)} n^2 dn. \quad (12c)$$

It should be noted that the transverse shear stiffness quantities are modified as:

$$A_{lm} = \sum_{k=1}^N k_{lm}^2 \bar{Q}_{lm}^{(k)} (n_{(k)} - n_{(k-1)}), \quad (l, m = 4, 5), \quad (13a)$$

where

$$k_{lm}^2 = k = \frac{5}{6}. \quad (13b)$$

There are many different parameters that affect the shear correction factor. However, in the present work, the shear factor value is chosen to be 5/6 as it is proposed by Reissner [8] and also reported by Librescu and Song [7], Ochoa and Reddy [9], and Vinson and Sierakowski [10]. Certainly more accurate methods may be used to calculate the shear correction factors, for instance, using a parabolic distribution of transverse shear stresses across the laminate thickness [7, 10]. Definitely the assumption of 5/6 for the shear correction factor may introduce some errors to the obtained results, which are inevitably accepted by the authors.

2.3. Equations of Motion

By the use of Extended Hamilton's Principle, the governing equations of motion of a thin-walled composite beam with a circumferentially asymmetric stiffness (CAS), i.e., $\theta(y) = -\theta(-y)$, $\theta(x) = -\theta(-x)$, where θ is the ply angle is developed in Song and Librescu [1], Qin and Librescu [5], and Qin [11] as:

$$\delta v_0 : a_{55}(v_0'' + \theta_x') + a_{56}\varphi''' = b_1 \ddot{v}_0, \quad (14a)$$

$$\begin{aligned} \delta \varphi : a_{37}\theta_x'' + a_{77}\varphi'' - a_{56}(v_0''' + \theta_x'') - a_{66}\varphi^{(IV)} \\ = (b_4 + b_5)\ddot{\varphi} - (b_{10} + b_{18})\ddot{\varphi}'', \end{aligned} \quad (14b)$$

$$\delta \theta_x : a_{33}\theta_x'' + a_{37}\varphi'' - a_{55}(v_0' + \theta_x) - a_{56}\varphi'' = (b_4 + b_{14})\ddot{\theta}_x, \quad (14c)$$

$$\delta u_0 : a_{14}w_0'' + a_{44}(u_0'' + \theta_y') = b_1 \ddot{u}_0, \quad (15a)$$

$$\delta w_0 : a_{11}w_0'' + a_{14}(u_0'' + \theta_y') = b_1 \ddot{w}_0, \quad (15b)$$

$$\begin{aligned} \delta \theta_y : a_{22}\theta_y'' - a_{14}w_0' - a_{44}(u_0' + \theta_y) \\ = (b_5 + b_{15})\ddot{\theta}_y, \end{aligned} \quad (15c)$$

in which the coefficients a_{ij} and b_i are listed in Appendices D and F of Song and Librescu [1].

Boundary conditions of the above equations are as follows:

At $z = 0$:

$$v_0 = \theta_x = \varphi = \varphi' = 0, \quad (16a)$$

$$w_0 = u_0 = \theta_y = 0. \quad (16b)$$

At $z = L$:

$$\delta v_0 : a_{55}(v_0' + \theta_x) + a_{56}\varphi'' = 0,$$

$$\delta \theta_x : a_{33}\theta_x' + a_{37}\varphi' = 0,$$

$$\begin{aligned} \delta \varphi : -a_{66}\varphi''' + a_{77}\varphi' - a_{56}(v_0'' + \theta_x') \\ + a_{37}\theta_x' + (b_{10} + b_{18})\ddot{\varphi}' = 0, \end{aligned}$$

$$\delta \varphi' : a_{56}(v_0' + \theta_x) + a_{66}\varphi'' = 0. \quad (17a)$$

$$\delta w_0 : a_{11}w_0' + a_{14}(u_0' + \theta_y) = 0,$$

$$\delta u_0 : a_{14}w_0' + a_{44}(u_0' + \theta_y) = 0,$$

$$\delta \theta_y : a_{22}\theta_y' = 0. \quad (17b)$$

Herein, v_0 denotes the vertical deflection, φ is the twist of the cross-section, θ_x is the rotation of the cross-section about x -axis, u_0 is the extensional deflection, w_0 is the lateral deflection, and θ_y is the rotation of the cross-section about y -axis. The coefficients a_{11} , a_{22} , a_{33} , a_{44} , a_{55} , a_{66} , and a_{77} denote the extensional, lateral bending, vertical bending, lateral transverse shear, vertical transverse shear, warping, and twist stiffness, respectively; a_{14} is the coefficient of elastic coupling between lateral transverse shear and lateral bending, a_{37} is the coefficient of elastic coupling between vertical bending and twist, and a_{56} is the coefficient of elastic coupling between vertical transverse shear and warping, while b_1 , b_4 , b_5 , b_{10} , b_{14} , b_{15} , and b_{18} are the inertia coefficients.

As stated in Qin and Librescu [5] and Qin [11], due to the complex boundary conditions and complex couplings involved in the above equations, the Extended Galerkin's Method (EGM) is used. The underlying idea of this method is to select weight functions that need only fulfill the geometric boundary conditions, while the effects of the natural boundary conditions are kept in the governing equations. When the linear combination of these weight functions is capable of satisfying the natural boundary conditions, the convergence rate is usually excellent. In the present analysis, a total number of nine shape functions in the form of simple polynomials are used. For the thin-walled beams to be investigated here, this method leads to both symmetric mass and stiffness matrices (further details can be found in Appendices B and C).

As mentioned earlier, Volovoi and Hodges [3] and also Jung et al [4] showed that the preliminary assumptions in constitutive equations have a significant and considerable effect on

the behavior of thin-walled composite beams, especially on predicting torsional stiffness of this kind of composite beams. They showed that, for a correct prediction of torsional stiffness, it is necessary for shell bending to be accounted for in the thin-walled composite beam model. To investigate the effects of preliminary assumptions for constitutive equations in free vibration behavior, three sets of assumptions will be examined here:

- (1) $\epsilon_{ss}^{(0)} = \epsilon_{ss}^{(1)} = 0$,
- (2) $N_{ss} = \epsilon_{ss}^{(1)} = 0$,
- (3) $N_{ss} = M_{ss} = 0$.

The three sets of assumptions introduced in the present work have been widely utilized in the static as well as free vibration analysis of thin-walled composite beams by different authors. For instance, the first set was used in Chandra and Chopra [2], Bauld et al. [12], and Chandra and Chopra [13]; the second set was used in Song and Librescu [1] and Centolanza et al. [14]; and the third set was used in Jung et al. [15], Wu and Sun [16], and Jung et al. [17]. The present study is carried out towards better understanding of the effects of these assumptions and also the assumption of in-plane rigidity of the beam cross-section on the free vibration behavior. These three sets of assumptions can be considered as the three levels of estimation of the elastic energy in the governing equations of motion and, consequently, the stiffness values of the beam cross-section.

The first set (i.e., $\epsilon_{ss}^{(0)} = \epsilon_{ss}^{(1)} = 0$) by ignoring any in-plane deformations of cross-section, as stated in Jung et al. [18] and Kosmatka and Ie [19], would be interpreted as neglecting the Poisson's effects. As a matter of fact, the in-plane cross-sectional deformations are results of Poisson's coupling with the out-of-plane cross-section stress distribution [19].

The second set (i.e., $N_{ss} = \epsilon_{ss}^{(1)} = 0$) results in the inevitable violation of compatibility and the equilibrium condition along the junction due to $N_{ss} = 0$. This loss of compatibility and lack of equilibrium can be justified on the following ground: the extensional stiffness of the constituent plates are so great in comparison to their flexural stiffness that little resistance is encountered as each of the plates moves in its own plane. The assumption of $\epsilon_{ss}^{(1)} = 0$ secures the in-plane rigidity condition of the cross section.

The third set (i.e., $N_{ss} = M_{ss} = 0$) is similar to the second set except for the fact that the in-plane rigidity condition of the cross-section (i.e., $\epsilon_{ss}^{(1)} = 0$) is relaxed by being replaced by ($M_{ss} = 0$), which means that little resistance is encountered as each of the plates bends in its plane.

Table 1. The lay-up configuration of thin-walled composite box-beams for the validation study

Lay-up	Upper wall	Lower wall	Left wall	Right wall
CAS1	[30] ₆	[30] ₆	[30/−30] ₃	[30/−30] ₃
CAS2	[45] ₆	[45] ₆	[45/−45] ₃	[45/−45] ₃

Table 2. Material properties and geometry of thin-walled composite box-beams

$E_{11} = 141.9$ GPa	$G_{12} = G_{13} = 6.0$ GPa
$E_{22} = E_{33} = 9.79$ GPa	$G_{23} = 4.83$ GPa
$\rho = 1445$ Kg/m ³	$\mu_{12} = \mu_{13} = 0.42, \mu_{23} = 0.25$
Length (L)	844.55 mm
Width (2b)	24.21 mm
Depth (2d)	13.46 mm
Thickness of each layer	0.127 mm

The above sets of assumptions will lead to the following sets of constitutive equations:

$$\begin{Bmatrix} N_{zz} \\ N_{sz} \\ M_{zz} \\ M_{sz} \\ N_{zn} \end{Bmatrix} = \begin{bmatrix} K_{11} & K_{12} & K_{13} & K_{14} & 0 \\ K_{21} & K_{22} & K_{23} & K_{24} & 0 \\ K_{41} & K_{42} & K_{43} & K_{44} & 0 \\ K_{51} & K_{52} & K_{53} & K_{54} & 0 \\ 0 & 0 & 0 & 0 & K_{65} \end{bmatrix} \begin{Bmatrix} \epsilon_{zz}^{(0)} \\ \gamma_{sz}^{(0)} \\ \phi' \\ \epsilon_{zz}^{(1)} \\ \gamma_{zn} \end{Bmatrix}. \quad (18)$$

The reduced stiffness coefficients (K_{ij}) corresponding to each set are listed in Appendix A.

3. Results and Discussions

Initially, the validation of the theoretical developments is attempted to ensure the proper implementation of the methodology and the corresponding assumptions in the constitutive equations. This is achieved by obtaining the results for a composite box-beam based on the third set of assumptions given above, and comparing the results with those already available in the literature, which are obtained by an experimental test [20] or other theoretical studies [5, 21, 22]. Two cases with CAS lay-up configurations, which are denoted by CAS1 and CAS2 (see Table 1), are considered. Table 2 shows the geometric dimensions and material properties used in the corresponding box-beams.

In order to study the effects of three different sets of constitutive equations on the free vibration behavior of thin-walled composite box-beams, two cases of lay-up configurations referred to as CAS3 and CAS4 with varying ply angles are considered. These lay-ups have initially been introduced by Volovoi and Hodges [3]. The stacking sequences of these lay-ups are given in Table 3 and the material properties and geometric dimensions used in the analysis are listed in Table 2. The predicted results by different sets of assumptions are compared with finite element method (FEM) results that are

Table 3. Thin-walled composite box-beams lay-ups

Lay-up	Upper wall	Lower wall	Left wall	Right wall
CAS3	[$\theta_3 / -\theta_3$] ₆	[$\theta_3 / -\theta_3$] ₆	[$\theta_3 / -\theta_3$] ₃	[$\theta_3 / -\theta_3$] ₃
CAS4	[θ] ₆	[θ] ₆	[$\theta / -\theta$] ₃	[$\theta / -\theta$] ₃

Table 4a. The experimental, FEM, and theoretical natural frequencies (Hz) for thin-walled composite box-beams

Lay-up	Mode No.	Ref. [20] (experiment)	Ref. [5]	Ref. [21]	Ref. [22]	Present (theory)	Present (FEM)
CAS1	1	20.96	21.8	19.92	22.07	22.3	20.965
	2	128.36	123.28	124.73	138.21	139.36	131.00
CAS2	1	16.67	15.04	14.69	15.13	15.28	15.372
	2	96.15	92.39	92.02	94.83	95.62	96.158

Table 4b. The relative differences in comparison with the either experiments or FEM analysis

Difference (experiment)							
Lay-up	Mode	Ref. [20] (experiment)	Ref. [5]	Ref. [21]	Ref. [22]	Present (theory)	Present (FEM)
CAS1	1TV*	—	4%	-4.96%	5.27%	6.4%	0.02%
	2TV	—	-3.96%	-2.83%	7.67%	8.53%	2.05%
CAS2	1TV	—	-9.78%	-11.9%	-9.24%	-8.33%	-7.8%
	2TV	—	-3.91%	-4.3%	-1.38%	-0.55%	0.008%
Difference (FEM)							
Lay-up	Mode	Ref. [20]	Ref. [5]	Ref. [21]	Ref. [22]	Present (theory)	Present (FEM)
CAS1	1TV	—	3.98%	-4.98%	5.27%	6.37%	—
	2TV	—	-5.9%	-4.78%	5.5%	6.38%	—
CAS2	1TV	—	-2.16%	-4.43%	-1.57%	-0.6%	—
	2TV	—	-3.91%	-4.3%	-1.38%	-0.56%	—

*Twist-vertical bending coupling modes [21].

obtained by implementing an ANSYS code using Shell99 element type.

It is noted that in the case of CAS1 and CAS2 lay-ups, for the sake of consistency with the literature notation, the ply angle θ is measured relative to “z” axis but for the CAS3 and

CAS4 it is measured with respect to “s” axis. Thus, the CAS1 and CAS2 lay-ups are identical to the CAS4 configuration when $\theta = 60^\circ$ and $\theta = 45^\circ$, respectively.

The validation results are presented in Table 4a in conjunction with the present FEM analysis. In Table 4b, a comparison between the results and those obtained by either the

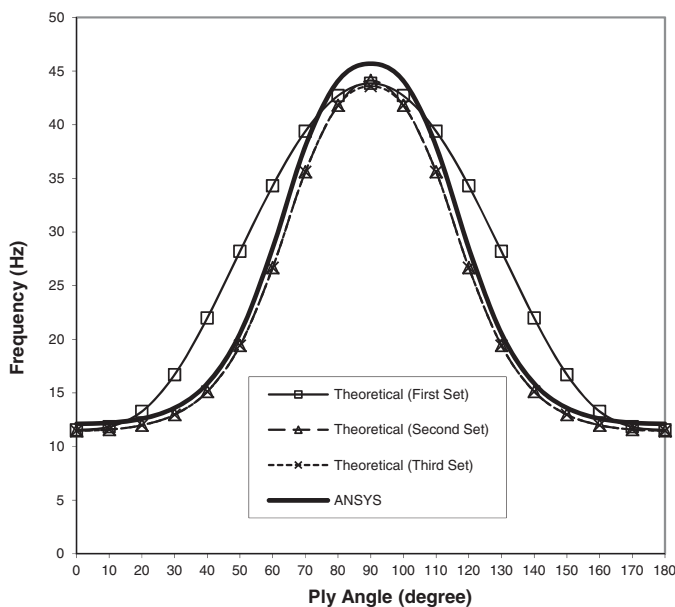


Fig. 3. The 1st natural frequency of the box-beam (CAS3).

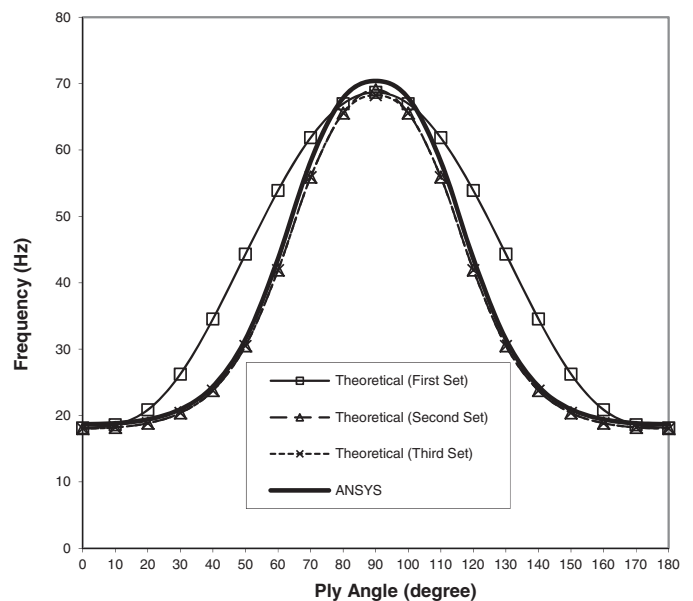


Fig. 4. The 2nd natural frequency of the box-beam (CAS3).

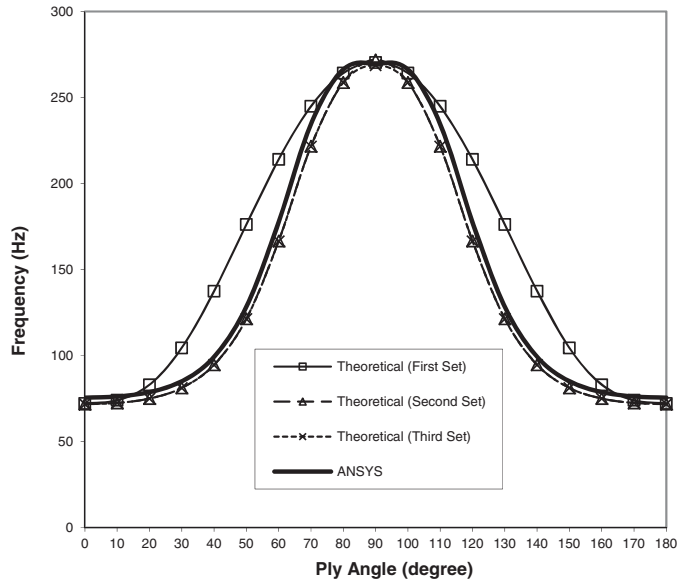


Fig. 5. The 3rd natural frequency of the box-beam (CAS3).

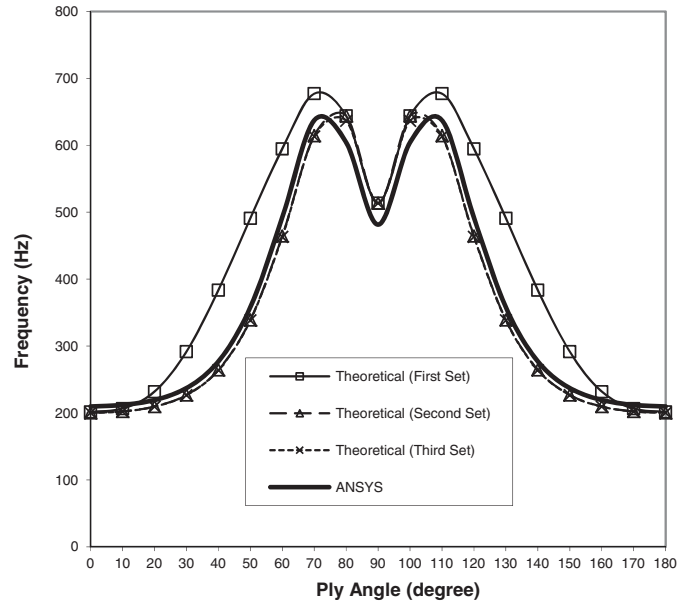


Fig. 7. The 5th natural frequency of the box-beam (CAS3).

experimental or FEM analysis is presented separately. As it is observed, the comparison of the results against experimental data does not follow a logical trend. This might be due to fact that the experimental results are usually affected by many practical factors, such as the accuracy of the implementation of the right boundary conditions, measurement errors, and many others. On the other hand, in the comparison of the present theoretical results as well as those of different references against the FEM results, a generally reasonable consistency can be observed. Further discussions, with respect to the comparison of the results, are provided

at a later stage in the article once the results corresponding to the effects of different sets of constitutive equations are presented.

Figures 3 through 9 display the first seven natural frequencies of CAS3 configuration. It is seen that the first set of assumptions ($\epsilon_{ss}^{(0)} = \epsilon_{ss}^{(1)} = 0$) have generally led to the results, which are not in close agreement with those predicted by FEM. The latter set of assumptions has mainly resulted in higher natural frequencies compared to those obtained by ANSYS. For example, in the case of $\theta = 50^\circ$, it is seen in

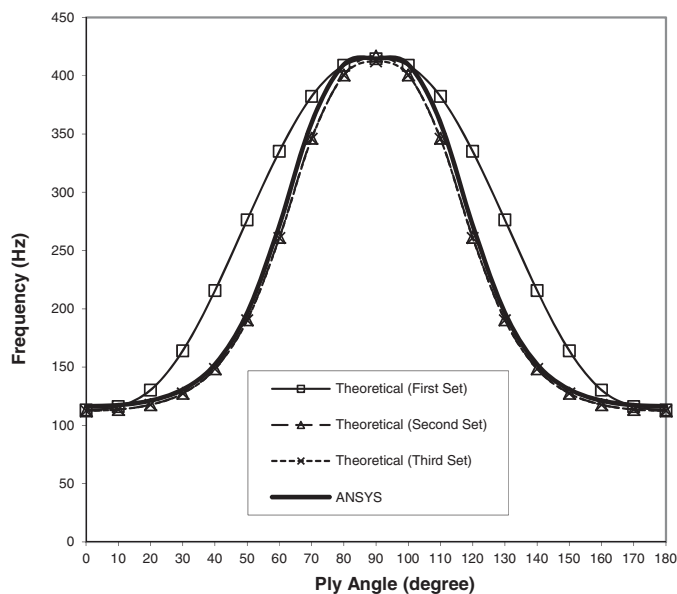


Fig. 6. The 4th natural frequency of the box-beam (CAS3).

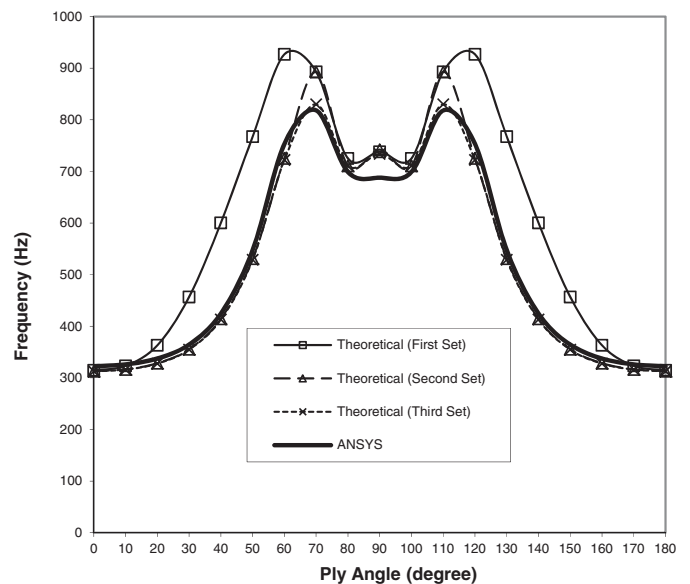


Fig. 8. The 6th natural frequency of the box-beam (CAS3).

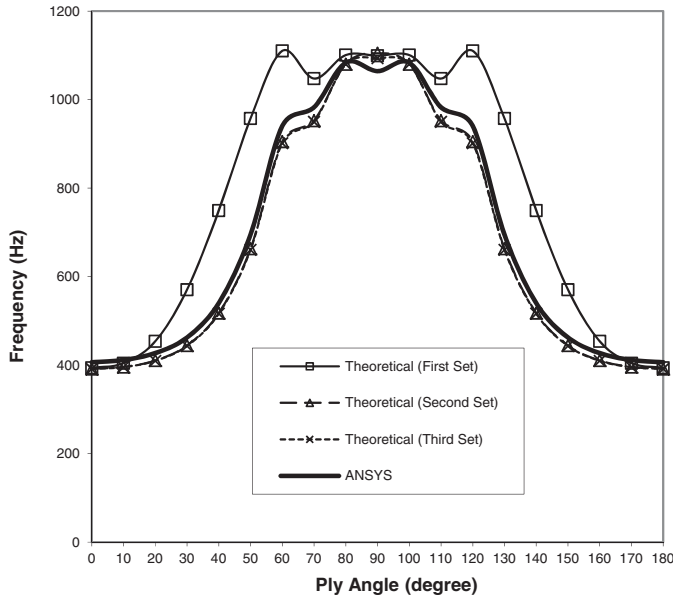


Fig. 9. The 7th natural frequency of the box-beam (CAS3).

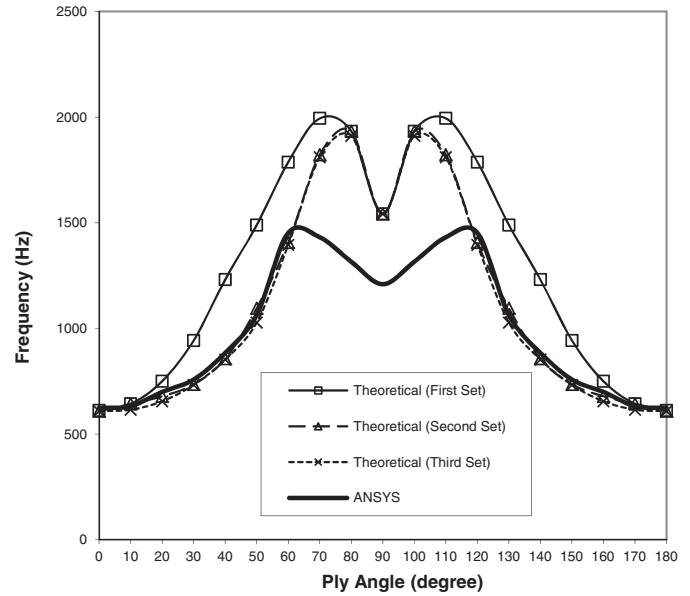


Fig. 11. The 9th natural frequency of the box-beam (CAS3).

Figure 3 that a difference of about 37% is experienced between the first natural frequency values obtained by either the first set of assumptions or by ANSYS code. It is also seen that the frequencies predicted by the second and third sets up to the 7th frequency are in very good agreement compared to FEM results. In the case of 8th and 9th (see Figures 10 and 11) frequencies for the ply angles of $0^\circ \leq \theta < 50^\circ$, the theoretical results obtained by the second and third sets are in a very close accordance compared to FEM results. However,

for the ply angles of $50^\circ \leq \theta < 90^\circ$, this accordance is not satisfying.

For CAS4 configuration, the predicted frequencies are depicted in Figures 12 through 20. Similar to that experienced with reference to CAS3 configuration, it is seen that in the case of CAS4 configuration, the natural frequencies are not predicted accurately based on the first set of assumptions (see Figures 12 through 20). For example, in the case of $\theta = 50^\circ$, it is seen in Figure 12 that a difference of about 68% is experienced between the first natural frequency values obtained by either the first set of assumptions or by ANSYS code.

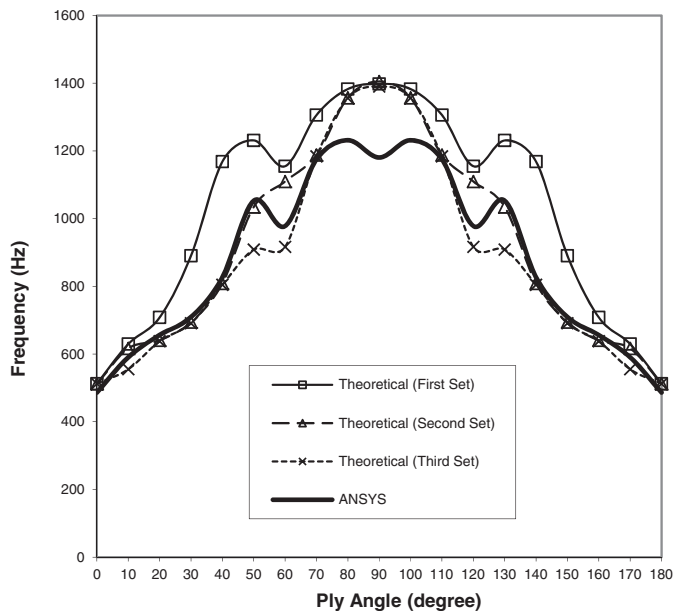


Fig. 10. The 8th natural frequency of the box-beam (CAS3).

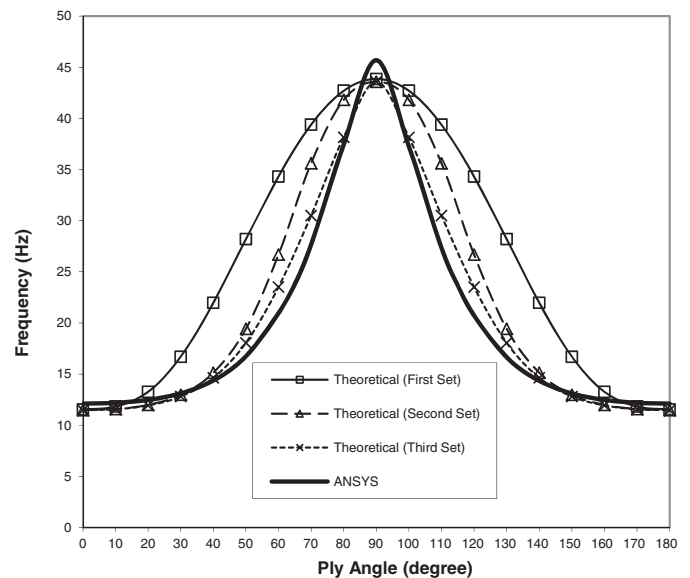


Fig. 12. The 1st natural frequency of the box-beam (CAS4).

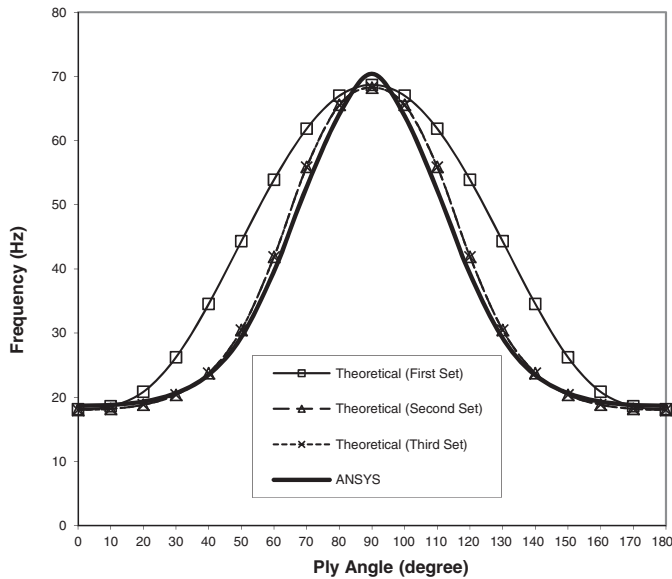


Fig. 13. The 2nd natural frequency of the box-beam (CAS4).

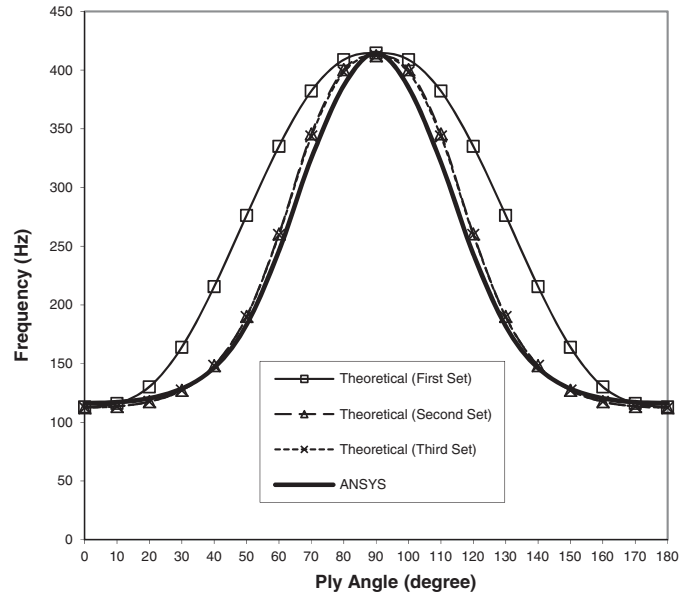


Fig. 15. The 4th natural frequency of the box-beam (CAS4).

Compared to the first set, the second set ($N_{ss} = \epsilon_{ss}^{(1)} = 0$), which is used by Librescu and his co-workers in free vibration and aeroelastic analyzes [23, 24], has generally predicted the results considerably closer to the FEM results. But the second set has also demonstrated noticeable errors in some cases. For example, in the case of $\theta = 70^\circ$, the first natural frequency (see Figure 12) is predicted with about 29% difference between that obtained by the second set and that achieved by FEM analysis. As far as the third set is concerned, it is seen that for the ply angles of $0^\circ \leq \theta < 50^\circ$ the natural frequencies up to the 7th frequency are predicted with a very good accuracy

compared to FEM results. For the ply angles of $50^\circ \leq \theta < 80^\circ$ in a number of modes, namely, the 1st, 3rd, 5th, 6th, and 7th, this accuracy starts to slightly deteriorate but it is still within the acceptable range. On the other hand, in the higher modes, namely, the 8th and 9th natural frequencies, the theoretical results compared to those of FEM are not satisfactory at all even in the case of the third set.

It seems that the above-mentioned free vibration behavior of composite box-beam occurred due to the preliminary assumptions that are made in developing the thin-walled composite beam model by which it is assumed that the beam

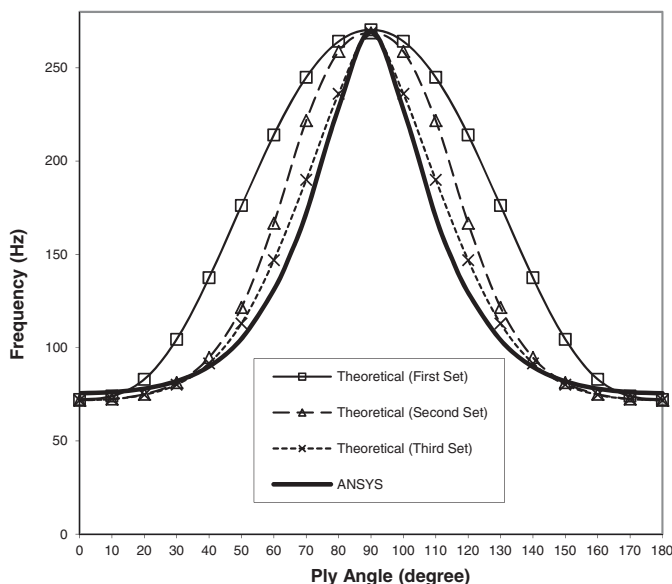


Fig. 14. The 3rd natural frequency of the box-beam (CAS4).

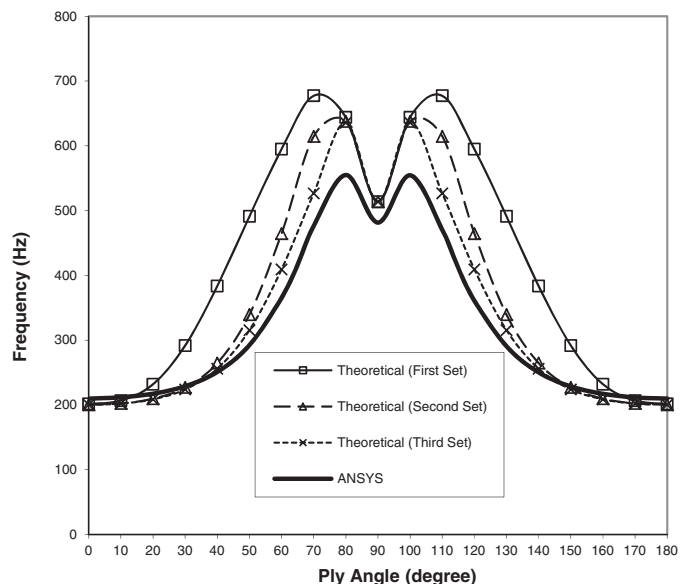


Fig. 16. The 5th natural frequency of the box-beam (CAS4).

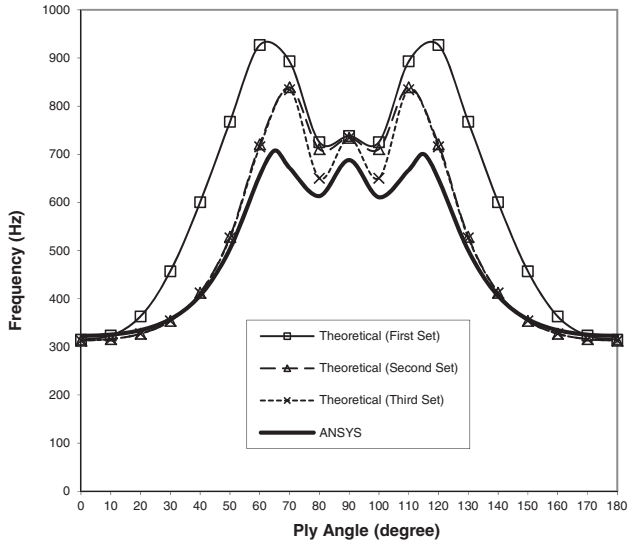


Fig. 17. The 6th natural frequency of the box-beam (CAS4).

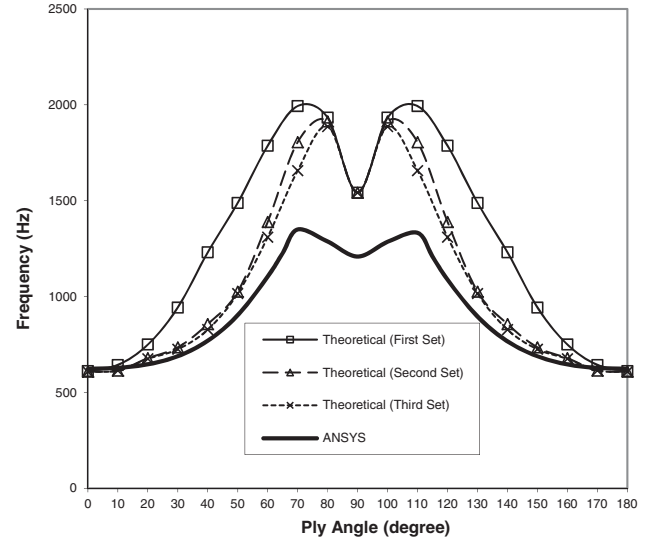


Fig. 20. The 9th natural frequency of the box-beam (CAS4).

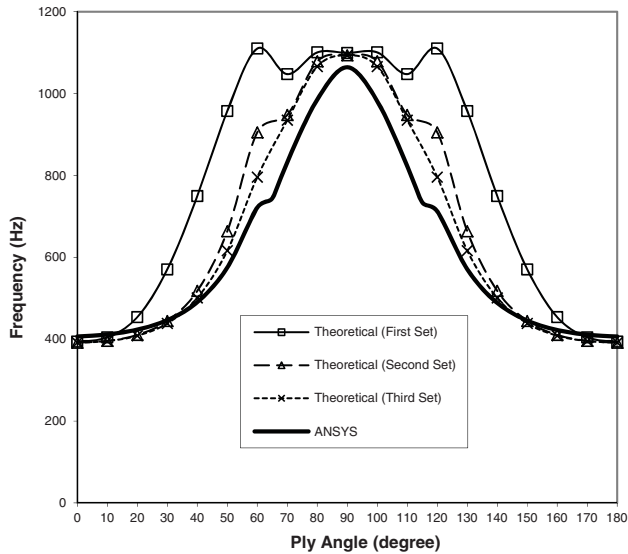


Fig. 18. The 7th natural frequency of the box-beam (CAS4).

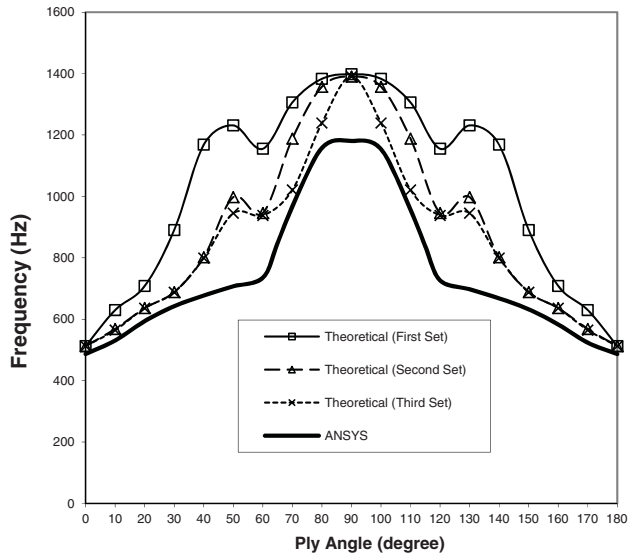


Fig. 19. The 8th natural frequency of the box-beam (CAS4).

cross-section does not deform in its own plane and also the magnitude of stiffness coefficient terms. This conclusion can be drawn by considering Figures 21 through 24. In Figures 21 and 22, the third and ninth ANSYS mode shapes for the CAS4 in

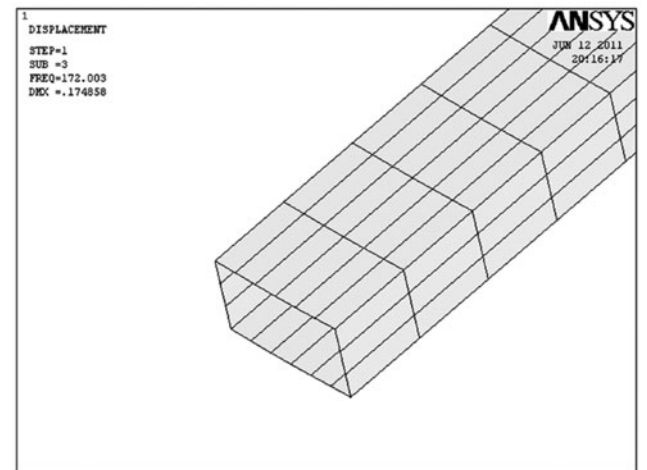
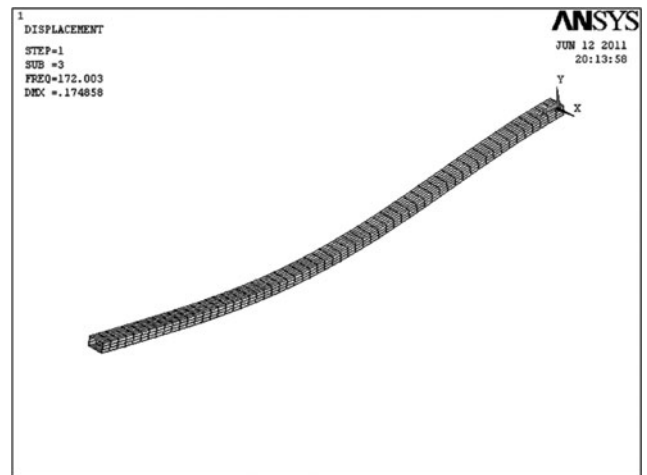


Fig. 21. ANSYS result for the 3rd mode shape of CAS4 ($\theta = 70^\circ$).

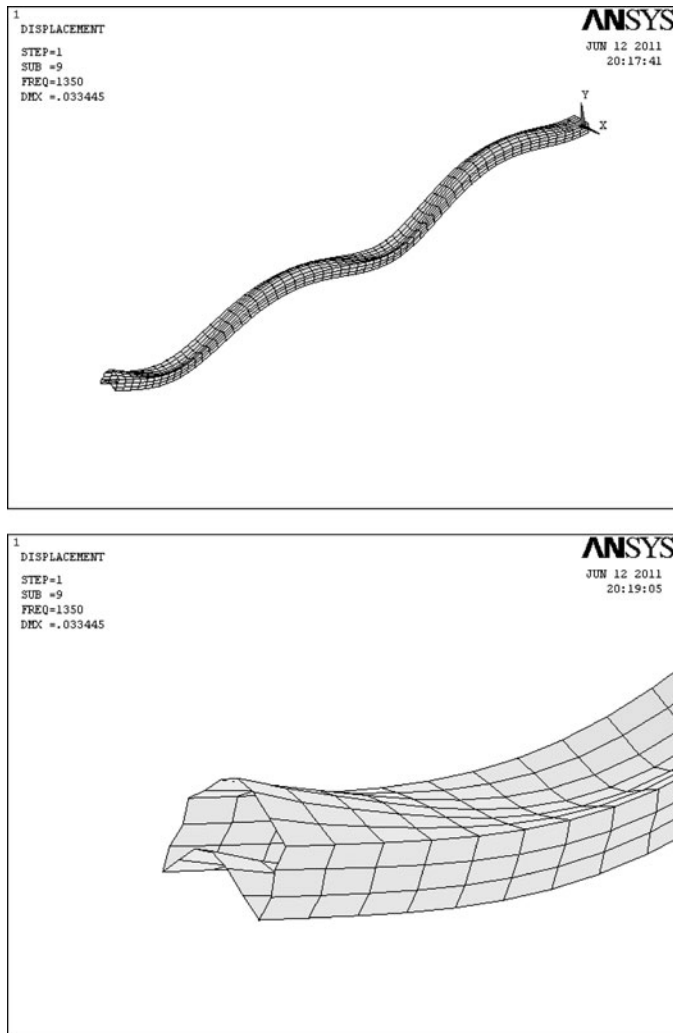


Fig. 22. ANSYS result for the 9th mode shape of CAS4 ($\theta = 70^\circ$).

the case of $\theta = 70^\circ$ are depicted, respectively. It is seen in Figure 22 corresponding to the ninth mode that the cross-section has significantly deformed in its plane (i.e., the shell bending has occurred), thus the developed thin-walled composite beam model being unable to capture the effects of cross-section deformation has not managed to follow the ANSYS analysis. A similar issue has also been addressed by Dancila et al. [25] who suggested that the higher natural frequencies cannot be predicted accurately unless the cross-sectional deformation is allowed for.

Figures 23 and 24 show the variation of transverse bending rigidity (a_{33}) and bending-torsion elastic coupling coefficient (a_{37}) with the ply angle based on the third set of assumptions for the CAS4 and CAS3 configurations, respectively.

It is seen in Figure 23 that for the CAS4 lay-up, the bending-twist elastic coupling coefficient has a notable size, which cannot be easily overlooked when compared to the bending rigidity and it has its maximum value for the ply angles of $50^\circ < \theta \leq 80^\circ$. Therefore, the contribution of twist modes in the natural frequencies is expected to be relatively significant within the aforementioned range of ply angles. This contribu-

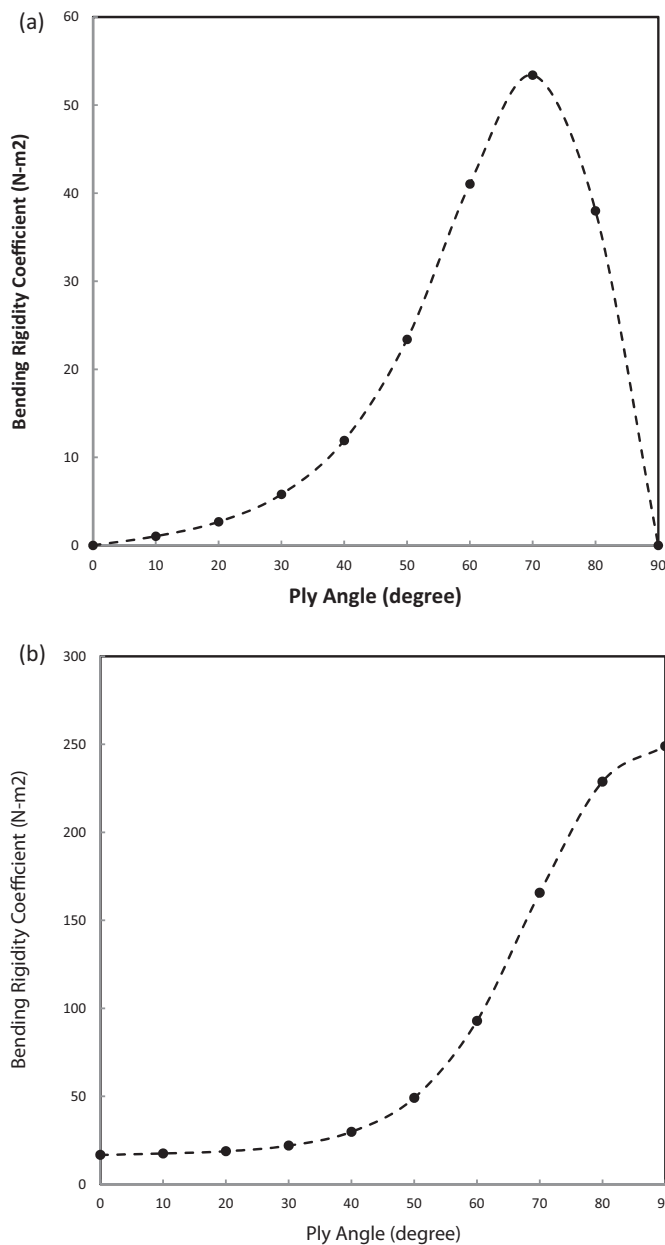


Fig. 23. (a) Bending-Twist Elastic Coupling Coefficient (CAS4) based on the third set (b) Bending Rigidity Coefficient (CAS4) based on the third set.

tion becomes even more pronounced in the case of higher natural frequencies where the twist deformation becomes apparent in the modes shapes (see Figure 22). Thus, in the case of lower natural frequencies and for the ply angles of $0^\circ < \theta \leq 50^\circ$ the results obtained by the present work are in a very good agreement compared to FEM results (see Figures 12–18 for the third set). Since the present model cannot capture the twist modes thoroughly (i.e., the in-plane shell bending modes are not captured) the predicted natural frequencies start to slightly lose their accuracy compared to FEM results in the case of the lower natural frequencies and for the ply angles of $50^\circ < \theta \leq 80^\circ$, in which the bending modes are still dominant

but the amount of bending-twist coupling is considerable (see Figures 12–18 for the third set).

Based on the above discussion and the fact that the CAS1 lay-up corresponds to CAS4 configuration with $\theta = 60^\circ$, the differences between the natural frequencies obtained by present theoretical results and those achieved by FEM analysis in the case of CAS1 lay-up (see Table 4b) are justified.

In the case of CAS3 lay-up as seen in Figure 24, the bending-twist coupling coefficient is not considerable relative to bending rigidity coefficient. Thus, for almost all ply angles in the case of lower modes (i.e., the first seven natu-

ral frequencies) where the twist and shell bending deformations are not yet dominant in the corresponding mode shape, the obtained results by using the third set are in close agreement with those obtained from the FEM analysis (see Figures 3–9).

4. Conclusions

The effects of different assumptions of constitutive equations on the free vibration behavior of a number of thin-walled composite beams with torsion-bending coupling have been investigated. The thin-walled composite beam model that is used in the present study is based on an existing beam model, including some non-classical effects, such as restrained warping and transverse shear. The free vibration results were presented for three sets of assumptions for constitutive equations and compared against finite element results provided using ANSYS. It is shown in this work that the assumptions of constitutive equations play an important role in predicting the natural frequencies of composite beams. Thus, an inappropriate selection of the corresponding assumptions may lead to catastrophic results. For example, in some cases a difference of about 68% compared to FEM results has been observed. As far as the lower natural frequencies are concerned, a good agreement has been observed between FEM results and those obtained by the application of the third set of assumptions. However, neither the third set nor the other sets of assumptions could capture the higher natural frequencies with adequate accuracy. It seems that the incorporation of cross-sectional deformation in the beam model is essential in order to be able to capture the higher natural frequencies.

References

- [1] O. Song and L. Librescu, Free vibration of anisotropic composite thin-walled beams of closed cross-section contour, *J. Sound Vib.*, vol. 167, no. 1, pp. 129–147, 1993.
- [2] R. Chandra and I. Chopra, Structural behavior of two-cell composite rotor blades with elastic couplings, *AIAA J.*, vol. 30, no. 12, pp. 2914–2921, 1992.
- [3] V.V. Volovoi and D.H. Hodges, Single- and multi-celled composite thin-walled beams, *AIAA J.*, vol. 40, no. 5, pp. 960–966, 2002.
- [4] S.N. Jung, V.T. Nagaraj, and I. Chopra, Refined structural model for thin- and thick-walled composite rotor blade, *AIAA J.*, vol. 40, no. 1, pp. 105–116, 2002.
- [5] Z. Qin and L. Librescu, On a shear-deformable theory of anisotropic thin-walled beams: Further contribution and validations, *Compos. Struct.*, vol. 56, pp. 345–358, 2002.
- [6] J.K. Suresh and V.T. Nagaraj, Higher-order shear deformation theory for thin-walled composite beams, *J. Aircraft*, vol. 33, no. 5, pp. 978–986, 1996.
- [7] L. Librescu and O. Song, *Thin-Walled Composite Beams: Theory and Application*, Springer Dordrecht, the Netherlands, 2006.
- [8] E. Reissner, On a variational theorem in elasticity, *J. Math. Phys.*, vol. 29, no. 2, pp. 90–95, 1950.
- [9] O.O. Ochoa and J.N. Reddy, *Finite Element Analysis of Composite Laminates*, Kluwer Academic Publishers, Dordrecht, The Netherlands, 1992.
- [10] J.R. Vinson and R.L. Sierakowski, *The Behavior of Structures Composed of Composite Materials*, Kluwer Academic Publishers, Dordrecht, The Netherlands, 2002.

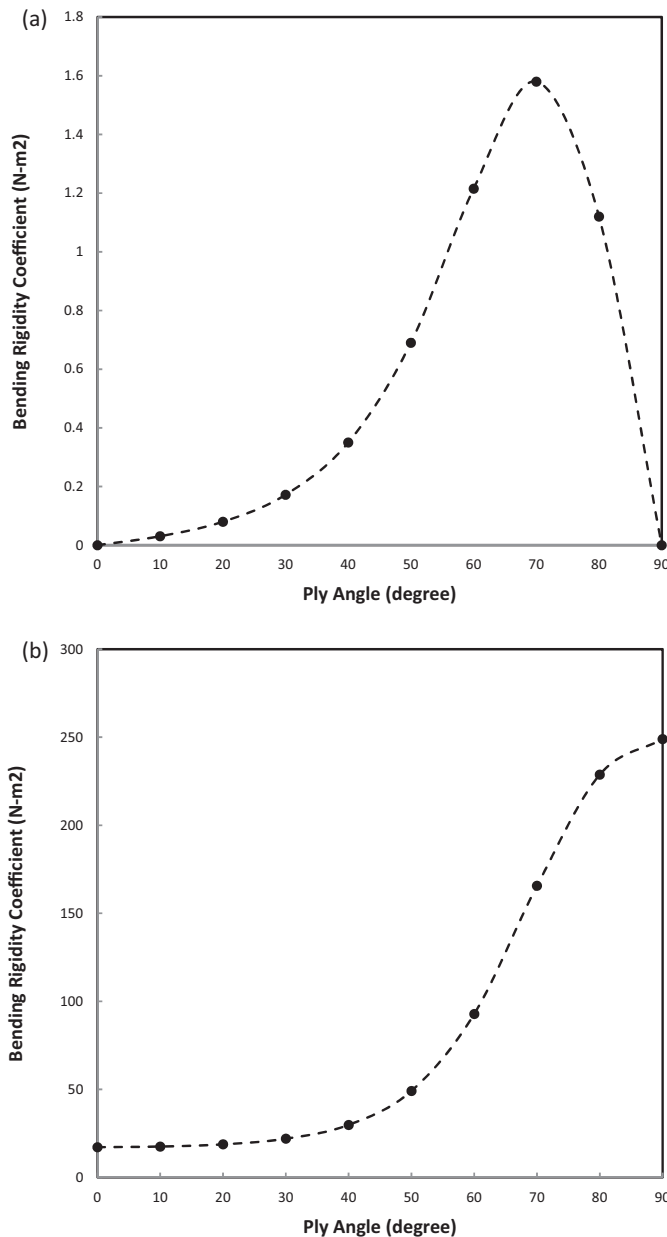


Fig. 24. (a) Bending-twist elastic coupling coefficient (CAS3) based on the third set. (b) Bending rigidity coefficient (CAS3) based on the third set.

- [11] Z. Qin, *Vibration and Aeroelasticity of Advanced Aircraft Wings Modeled as Thin-Walled Beams-Dynamics, Stability and Control*, Ph.D. Thesis, Virginia Polytechnic Institute and State University, Blacksburg, VA, 2001.
- [12] N.R. Bauld, L.S. Tzeng, and A. Vlasov, Theory for fiber-reinforced beams with thin-walled open cross sections, *Int. J. Solids Struct.*, vol. 20, no. 3, pp. 277–297, 1984.
- [13] R. Chandra and I. Chopra, Experimental and theoretical analysis of composite i-beams with elastic couplings, *AIAA J.*, vol. 29, no. 12, pp. 2197–2206, 1991.
- [14] L.R. Centolanza, E.C. Smith, and B. Kumar, Refined structural modeling and structural dynamics of elastically tailored composite rotor blades, *Proceedings of the 37th AIAA/ASME/ASCE/AHS/ASC Structures, Structural Dynamics, and Materials Conference and Exhibit*, pp. 2002–2012, April 15–17, Salt Lake City, UT, 1996.
- [15] S.N. Jung, I.J. Park, and E.S. Shin, Theory of thin-walled composite beams with single and double-cell sections, *Composites Part B: Eng.*, vol. 38, no. 2, pp. 182–192, 2007.
- [16] X.X. Wu and C.T. Sun, Vibration analysis of laminated composite thin-walled beams using finite elements, *AIAA J.*, vol. 29, no. 5, pp. 736–742, 1990.
- [17] S.N. Jung, V.T. Nagaraj, and I. Chopra, Refined structural dynamics model for composite rotor blades, *AIAA J.*, vol. 39, no. 2, pp. 339–348, 2001.
- [18] S.N. Jung, V.T. Nagaraj, and I. Chopra, Assessment of composite rotor blade modeling techniques, *J. Am. Helicopter Soc.*, vol. 44, no. 3, pp. 188–205, 1999.
- [19] J.B. Kosmatka and C. Ie, On the vibration behavior of shear-deformable prismatic beams including in-plane cross-section deformation, *Proceedings of the 32nd AIAA/ASME/ASCE/AHS/ASC Structures, Structural Dynamics and Material Conference*, pp. 1462–1474, April 8–10, Baltimore, MD, 1991.
- [20] R. Chandra and I. Chopra, Experimental-theoretical investigation of the vibration characteristics of rotating composite box-beams, *J. Aircraft*, vol. 29, no. 4, pp. 657–664, 1992.
- [21] E.A. Armanios and A.M. Badir, Free vibration analysis of anisotropic thin-walled closed-section beams, *AIAA J.*, vol. 33, no. 10, pp. 1905–1910, 1995.
- [22] T.P. Vo and J. Lee, Free vibration of thin-walled composite box beams, *Compos. Struct.*, vol. 84, no. 1, pp. 11–20, 2008.
- [23] Z. Qin, P. Mazocca, and L. Librescu, Aeroelastic instability and response of advanced aircraft wings at subsonic flight speeds, *Aerospace Sci. Technol.*, vol. 6, no. 3, pp. 195–208, 2002.
- [24] Z. Qin and L. Librescu, Aeroelastic instability of aircraft wings modeled as anisotropic composite thin-walled beams in incompressible flow, *J. Fluids Struct.*, vol. 18, no. 1, pp. 43–61, 2003.
- [25] D.S. Dancila, E.A. Armanios, and W.K. Lentz, Free vibration of thin-walled closed-section composite beams with optimum and near-optimum coupling, *J. Thermoplastic Compos. Mater.*, vol. 12, no. 1, pp. 2–12, 1999.

Appendix A

The reduced stiffness coefficients for $N_{ss} = M_{ss} = 0$:

$$K_{11} = A_{22} + (A_{12}^2 D_{11} - 2A_{12} B_{11} B_{12} + B_{12}^2 A_{11}) / (B_{11}^2 - D_{11} A_{11}),$$

$$K_{12} = A_{26} + [A_{12} (A_{16} D_{11} - B_{11} B_{16}) + B_{12} (A_{11} B_{16} - B_{11} A_{16})] / (B_{11}^2 - D_{11} A_{11}),$$

$$K_{13} = \Psi(s) K_{12},$$

$$K_{14} = B_{22} + [A_{12} (B_{12} D_{11} - B_{11} D_{12}) + B_{12} (A_{11} D_{12} - B_{11} B_{12})] / (B_{11}^2 - D_{11} A_{11}),$$

$$K_{21} = A_{26} + [A_{16} (A_{12} D_{11} - B_{11} B_{12}) + B_{16} (A_{11} B_{12} - B_{11} A_{12})] / (B_{11}^2 - D_{11} A_{11}),$$

$$K_{22} = A_{66} + (A_{16}^2 D_{11} - 2A_{16} B_{11} B_{16} + B_{16}^2 A_{11}) / (B_{11}^2 - D_{11} A_{11}),$$

$$K_{23} = \Psi(s) K_{22},$$

$$K_{24} = B_{26} + [A_{16} (B_{12} D_{11} - B_{11} D_{12}) + B_{16} (A_{11} D_{12} - B_{11} B_{12})] / (B_{11}^2 - D_{11} A_{11}),$$

$$K_{41} = B_{22} + [B_{12} (A_{12} D_{11} - B_{11} B_{12}) + D_{12} (A_{11} B_{12} - B_{11} A_{12})] / (B_{11}^2 - D_{11} A_{11}),$$

$$K_{42} = B_{26} + [B_{12} (A_{16} D_{11} - B_{11} B_{16}) + D_{12} (A_{11} B_{16} - B_{11} A_{16})] / (B_{11}^2 - D_{11} A_{11}),$$

$$K_{43} = \Psi(s) K_{42},$$

$$K_{44} = D_{22} + [B_{12}^2 D_{11} - 2B_{12} B_{11} D_{12} + D_{12}^2 A_{11}] / (B_{11}^2 - D_{11} A_{11}),$$

$$K_{51} = B_{26} + [B_{16} (A_{12} D_{11} - B_{11} B_{12}) + D_{16} (A_{11} B_{12} - B_{11} A_{12})] / (B_{11}^2 - D_{11} A_{11}),$$

$$K_{52} = B_{66} + [B_{16} (A_{16} D_{11} - B_{11} B_{16}) + D_{16} (A_{11} B_{16} - B_{11} A_{16})] / (B_{11}^2 - D_{11} A_{11}),$$

$$K_{53} = \Psi(s) K_{52},$$

$$K_{54} = D_{22} + [B_{16} (B_{12} D_{11} - B_{11} D_{12}) + D_{16} (A_{11} D_{12} - B_{11} B_{12})] / (B_{11}^2 - D_{11} A_{11}),$$

$$K_{65} = A_{44} - \frac{A_{45}^2}{A_{55}}.$$

The reduced stiffness coefficients for $N_{ss} = \varepsilon_{ss}^{(1)} = 0$:

$$K_{11} = A_{22} - \frac{A_{12}^2}{A_{11}},$$

$$K_{12} = A_{26} - \frac{A_{12} A_{16}}{A_{11}} = K_{21},$$

$$K_{13} = \left(A_{26} - \frac{A_{12} A_{16}}{A_{11}} \right) \Psi(s),$$

$$K_{14} = B_{22} - \frac{A_{12} B_{12}}{A_{11}} = K_{41},$$

$$K_{22} = A_{66} - \frac{A_{16}^2}{A_{11}},$$

$$K_{23} = \left(A_{66} - \frac{A_{16}^2}{A_{11}} \right) \Psi(s),$$

$$K_{24} = B_{26} - \frac{A_{16} B_{12}}{A_{11}} = K_{42},$$

$$K_{43} = \left(B_{26} - \frac{A_{16} B_{12}}{A_{11}} \right) \Psi(s),$$

$$K_{44} = D_{22} - \frac{B_{12}^2}{A_{11}},$$

$$K_{51} = B_{26} - \frac{B_{16} A_{12}}{A_{11}},$$

$$K_{52} = B_{66} - \frac{B_{16} A_{16}}{A_{11}},$$

$$K_{53} = \left(B_{66} - \frac{B_{16} A_{16}}{A_{11}} \right) \Psi(s),$$

$$K_{54} = D_{26} - \frac{B_{12} B_{16}}{A_{11}},$$

$$K_{65} = A_{44} - \frac{A_{45}^2}{A_{55}}.$$

The reduced stiffness coefficients for $\epsilon_{ss}^{(0)} = \epsilon_{ss}^{(1)} = 0$:

$$K_{11} = A_{22},$$

$$K_{12} = A_{26} = K_{21},$$

$$K_{13} = K_{12} \Psi(s),$$

$$K_{14} = B_{22} = K_{41},$$

$$K_{22} = A_{66},$$

$$K_{23} = K_{22} \Psi(s),$$

$$K_{24} = B_{26} = K_{42},$$

$$K_{43} = B_{26} \Psi(s),$$

$$K_{44} = D_{22},$$

$$K_{51} = B_{26},$$

$$K_{52} = B_{66},$$

$$K_{53} = B_{66} \Psi(s),$$

$$K_{54} = D_{26},$$

$$K_{65} = A_{44} - \frac{A_{45}^2}{A_{55}}.$$

Appendix B

In order to apply the EGM to the governing equations, the separation of variables is implemented as follows:

$$u_0(z, t) = \Psi_u^T(z) \mathbf{q}_u(t), \quad v_0(z, t) = \Psi_v^T(z) \mathbf{q}_v(t),$$

$$w_0(z, t) = \Psi_w^T(z) \mathbf{q}_w(t),$$

$$\varphi(z, t) = \Psi_\varphi^T(z) \mathbf{q}_\varphi(t), \quad \theta_x(z, t) = \Psi_x^T(z) \mathbf{q}_x(t),$$

$$\theta_y(z, t) = \Psi_y^T(z) \mathbf{q}_y(t).$$

where $\Psi_u^T(z), \Psi_v^T(z), \Psi_w^T(z), \Psi_\varphi^T(z), \Psi_x^T(z)$, and $\Psi_y^T(z)$ are appropriate shape functions and $\mathbf{q}_u(t), \mathbf{q}_v(t), \mathbf{q}_w(t), \mathbf{q}_\varphi(t), \mathbf{q}_x(t)$, and $\mathbf{q}_y(t)$ are the vectors of generalized coordinates. Applying the later equations results in the discretized equations of motion:

$$[M] \{\ddot{\mathbf{q}}\} + [K] \{\mathbf{q}\} = \{\mathbf{0}\},$$

where $\{\mathbf{q}\} = [\mathbf{q}_u^T \ \mathbf{q}_v^T \ \mathbf{q}_w^T \ \mathbf{q}_\varphi^T \ \mathbf{q}_x^T \ \mathbf{q}_y^T]^T$ and

$$M = \int_0^L \begin{bmatrix} b_1 \Psi_u \Psi_u^T & 0 & 0 & 0 & 0 & 0 \\ & b_1 \Psi_v \Psi_v^T & 0 & 0 & 0 & 0 \\ & & b_1 \Psi_w \Psi_w^T & 0 & 0 & 0 \\ & & & (b_4 + b_5) \Psi_\varphi \Psi_\varphi^T & 0 & 0 \\ & & & + (b_{10} + b_{18}) \Psi_\varphi' \Psi_\varphi'^T & 0 & 0 \\ & \text{Symmetric} & & & (b_4 + b_{14}) \Psi_x \Psi_x^T & 0 \\ & & & & & (b_5 + b_{15}) \Psi_y \Psi_y^T \end{bmatrix},$$

$$K = \int_0^L \begin{bmatrix} a_{44} \Psi_u' \Psi_u'^T & 0 & a_{14} \Psi_u' \Psi_w'^T & 0 & 0 & a_{44} \Psi_u \Psi_y'^T \\ & a_{55} \Psi_v' \Psi_v'^T & 0 & a_{56} \Psi_v' \Psi_\varphi'^T & a_{55} \Psi_v' \Psi_x^T & 0 \\ & & a_{11} \Psi_w' \Psi_w'^T & 0 & 0 & a_{14} \Psi_w' \Psi_y^T \\ & & & a_{77} \Psi_\varphi' \Psi_\varphi'^T + a_{66} \Psi_\varphi'' \Psi_\varphi''^T & (a_{37} - a_{56}) \Psi_\varphi' \Psi_x^T & 0 \\ & \text{Symmetric} & & & a_{55} \Psi_x \Psi_x^T + a_{33} \Psi_x' \Psi_x'^T & 0 \\ & & & & & a_{44} \Psi_y \Psi_y^T + a_{22} \Psi_y' \Psi_y'^T \end{bmatrix}.$$

In the present work, shape functions in the form of simple polynomials are adopted:

$$\begin{aligned} \psi_u^T(z) &= [z \ z^2 \ \dots \ z^N]^T, \psi_v^T(z) = [z \ z^2 \ \dots \ z^N]^T, \psi_w^T(z) = [z \ z^2 \ \dots \ z^N]^T, \\ \psi_\phi^T(z) &= [z^2 \ z^3 \ \dots \ z^{N+1}]^T, \psi_x^T(z) = [z \ z^2 \ \dots \ z^N]^T, \psi_y^T(z) = [z \ z^2 \ \dots \ z^N]^T, \end{aligned}$$

where N is the number of shape functions to be used in the analysis.

Appendix C

Convergence study of the EGM:

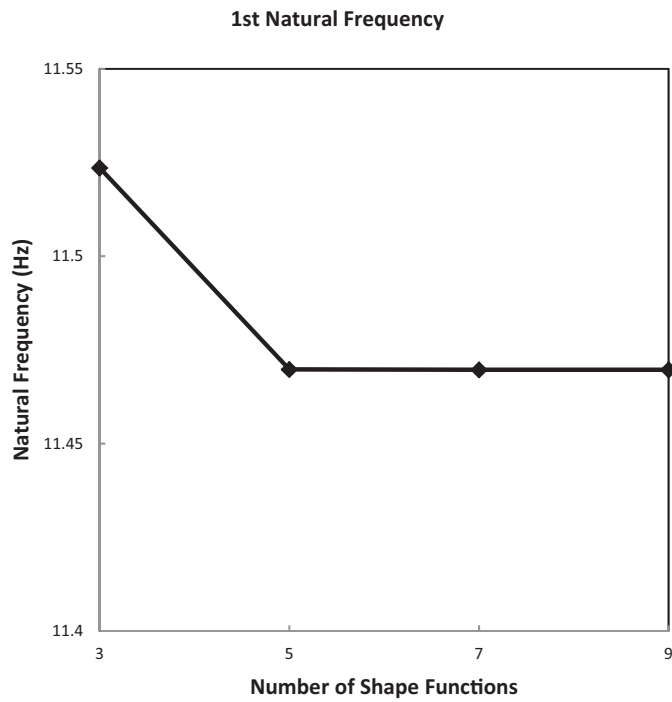


Fig. C1.

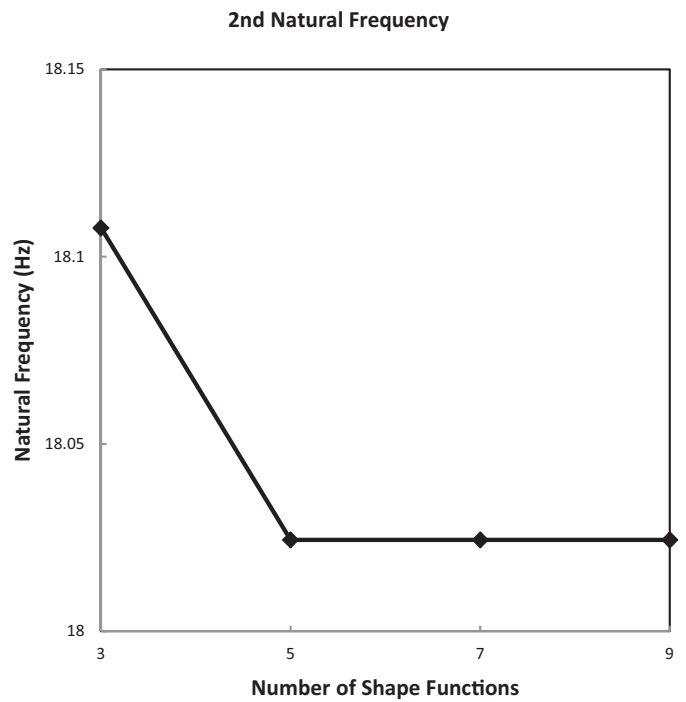


Fig. C2.

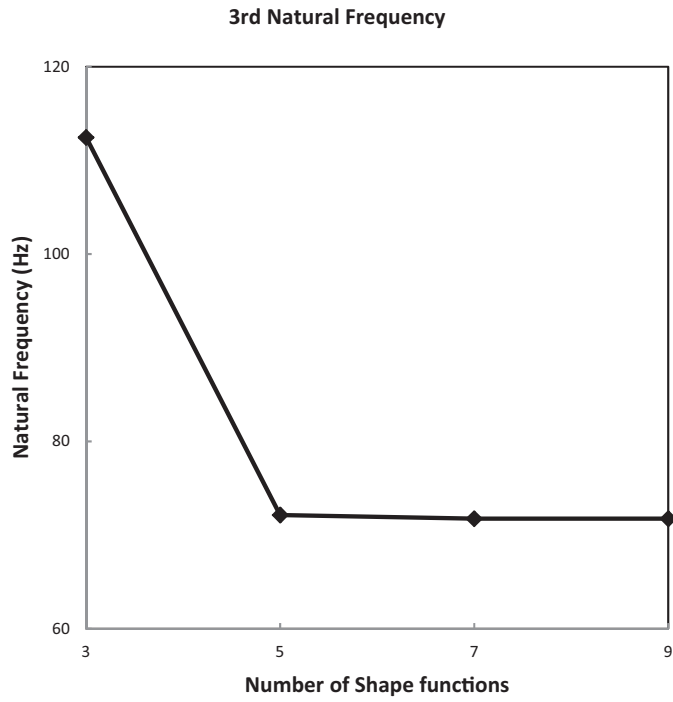


Fig. C3.

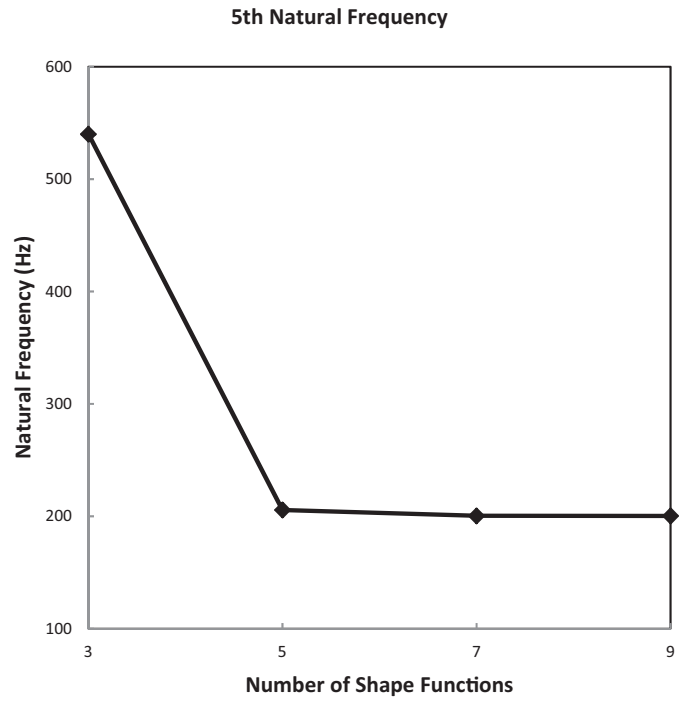


Fig. C5.

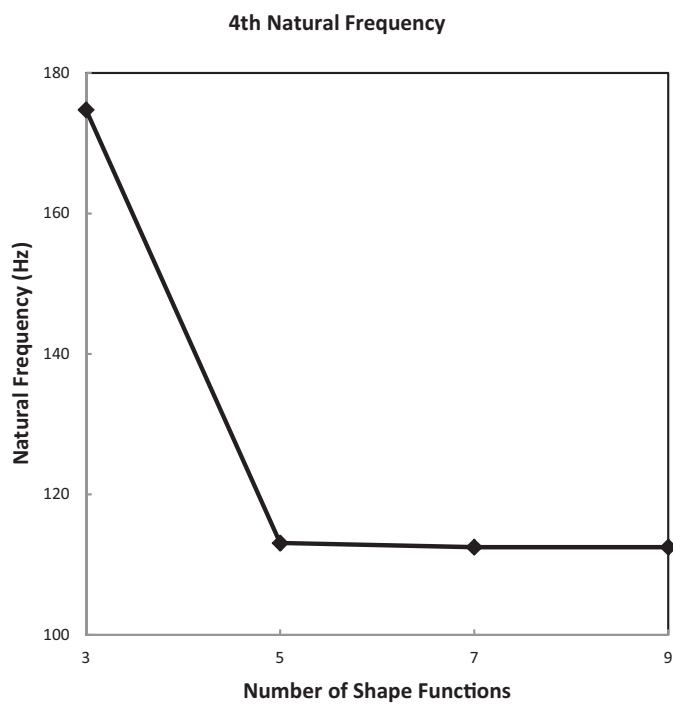


Fig. C4.

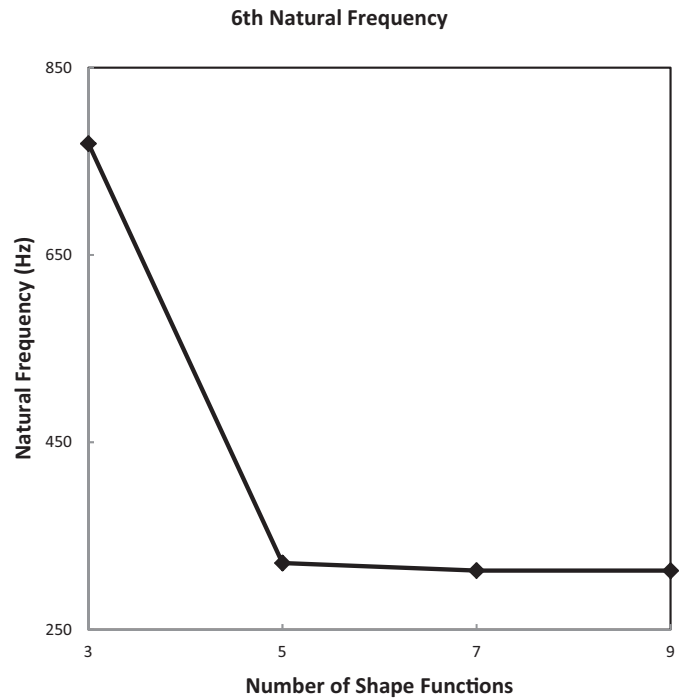


Fig. C6.

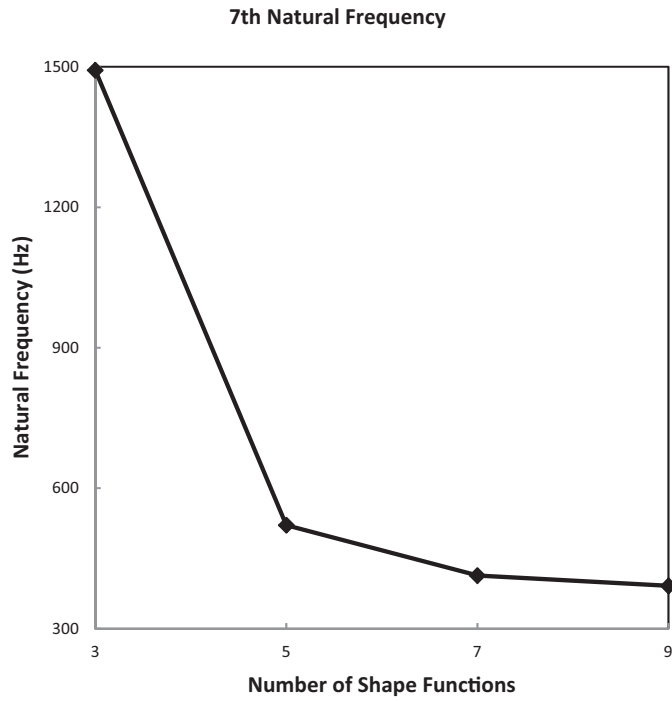


Fig. C7.

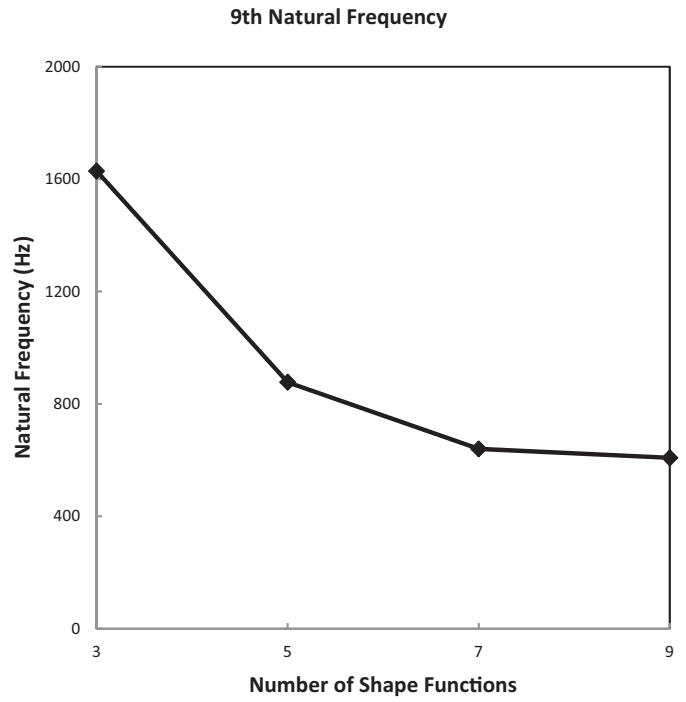


Fig. C9.

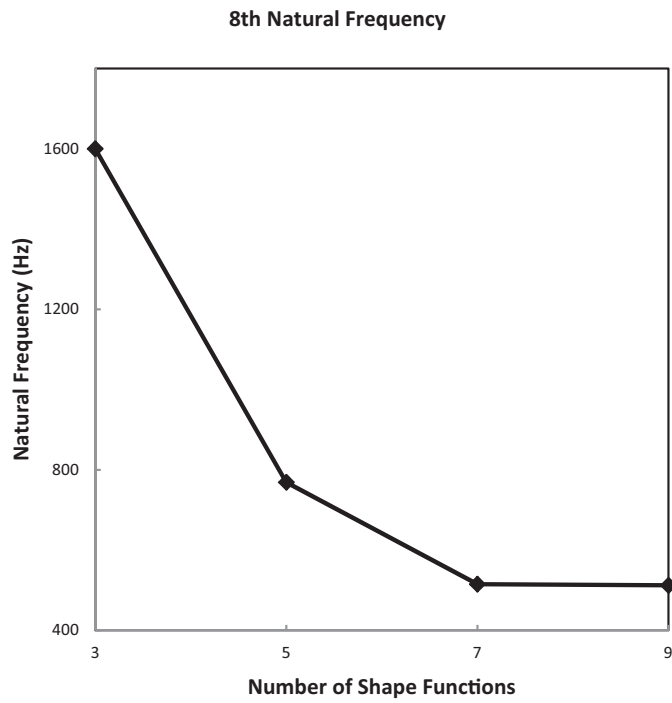


Fig. C8.

Convergence of the nine first natural frequencies of composite box-beam *CAS4*, $\theta = 0^\circ$.